Multifarious Biologic Loaded Liposomes that Stimulate the Mammalian Target of Rapamycin Signaling Pathway Show Retina Neuroprotection after Retina Damage

Eriksen, Anne Zebitz; Eliasen, Rasmus; Oswald, Julia; Kempen, Paul; Melander, Fredrik; Andresen, Thomas Lars; Young, Michael; Baranov, Petr; Urquhart, Andrew

Published in:
A C S Nano

Link to article, DOI:
10.1021/acsnano.8b00596

Publication date:
2018

Document Version
Publisher's PDF, also known as Version of record

ACS NANO

Cite This: ACS Nano 2018, 12, 7497−7508

www.acsnano.org

ARTICLE

Multifarious Biologic Loaded Liposomes that Stimulate the Mammalian Target of Rapamycin Signaling Pathway Show Retina Neuroprotection after Retina Damage

Anne Z. Eriksen,[†] Rasmus Eliasen,[†] Julia Oswald,[‡] Paul J. Kempen,[†] Fredrik Melander,[†] Thomas L. Andresen,[†] Michael Young,[‡] Petr Baranov,[‡] and Andrew J. Urquhart*,[†]

[†]DTU Nanotech, Department of Micro- and Nanotechnology, Technical University of Denmark, 2800 Kongens Lyngby, Denmark

[‡]Schepens Eye Research Institute, Massachusetts Eye and Ear, 20 Staniford Street, Boston, Massachusetts 02114, United States

Supporting Information

ABSTRACT: **A common event in optic neuropathies is the loss of axons and death of retinal ganglion cells (RGCs) resulting in irreversible blindness. Mammalian target of rapamycin (mTOR) signaling pathway agonists have been shown to foster axon regeneration and RGC survival in animal models of optic nerve damage. However, many challenges remain in developing therapies that exploit cell growth and tissue remodeling including (i) activating/inhibiting cell pathways synergistically, (ii) avoiding tumorigenesis, and (iii) ensuring appropriate physiological tissue function. These challenges are further exacerbated by the need to overcome ocular physiological barriers and clearance mechanisms. Here we present liposomes loaded with multiple mTOR pathway stimulating biologics designed to enhance neuroprotection after retina damage. Liposomes were loaded with ciliary neurotrophic factor, insulin-like growth factor 1, a lipopeptide N-fragment osteopontin mimic, and lipopeptide phosphatase tension homologue inhibitors for either the ATP domain or the c-terminal tail. In a mouse model of *N*-methyl-D-aspartic acid induced RGC death, a single intravitreal administration of liposomes reduced both RGC death and loss of retina electrophysiological function. Furthermore, combining liposomes with transplantation of induced pluripotent stem cell derived RGCs led to an improved electrophysiological outcome in mice. The results presented here show that liposomes carrying multiple signaling pathway modulators can facilitate neuroprotection and transplant electrophysiological outcome.**

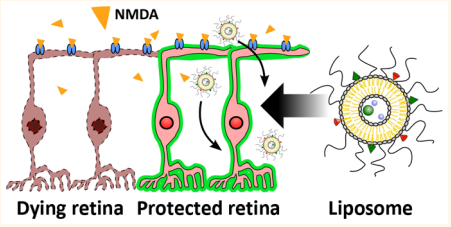

KEYWORDS: *retina, liposomes, neuropathy, neuroprotection, ganglion, transplant*

Optic neuropathies (*e.g.*, glaucoma, *etc.*) are a leading cause of irreversible blindness worldwide, impairing patient quality of life and posing a negative impact on socioeconomics.[1] A common event in optic neuropathies is the loss of RGC axons in both the optic nerve (ON) and retina, followed by the death of RGCs.[2,3] RGCs are responsible for signal transmission from the retina to the brain and RGC death through apoptosis[4] is associated with progressive loss of vision. Lack of regenerative capacity in the mammalian retina makes the loss of RGCs irreversible. Autologous nerve grafts for ON damage are undesirable due to excessive surgery (or unfeasible depending on location of damage) while retina transplantation for retina damage has had poor success.[5] Multiple factors contribute to neuronal loss in the retina including failure of axonal transport; toxic pro-neurotrophins; intrinsic and extrinsic activation of apoptotic signals; mitochondrial dysfunction; excitotoxic damage; oxidative stress; misbehaving reactive glia; loss of synaptic connectivity and neurotrophic factor (NF) deprivation.[6] The multifactorial nature of optic neuropathies would indicate that a combination therapy (*e.g.*, combined pharmacotherapies, pharmacotherapy, and cell therapy, *etc.*) linked to neuroprotection and/or nerve regeneration would significantly improve the outcome of optic neuropathies. This is indicated by previous studies either involving the supplementation of different neurotrophic factors to protect RGCs in different animal models (induced hypertension, ON transection and ON crush[7−13]) or the deletion of cell growth regulatory genes PTEN and SOCS3 to protect RGCs after axotomy.[14−16]

Arguably, the most striking results in axon regrowth after ON transection so far have been achieved by Bei *et al.* using a combination of adeno-associated virus (AAV) assisted overexpression of ciliary neurotrophic factor (CNTF), insulin-like growth factor 1 (IGF-1) and osteopontin (OPN), combined

Received: January 23, 2018
Accepted: July 13, 2018
Published: July 13, 2018

DOI: 10.1021/acsnano.8b00596
ACS Nano 2018, 12, 7497−7508

with AAV codeletion of PTEN and SOCS3 genes.[17] CNTF and IGF-1 have both been shown to promote axon regeneration by activation of the mTOR pathway.[4,17−20] The cytokine CNTF is capable of activating several different signaling pathways such as JAK-signal transducers, MAPK, PI3K, and mTOR-p70S6K by binding to receptors at the cell surface.[21] CNTF has been shown to stimulate mTOR activation of STAT3, hence implicating CNTF and mTOR as transcriptional regulators in neuroblastoma cells.[22] CNTF supplementation has also been shown to prevent the decrease in mTOR activity *in vitro* in RGCs.[23] IGF-1 is a protein hormone that binds to a receptor tyrosine kinases (IGF-1R) on the cell surface[24] activating PI3K.[25,26] IGF-1 and regulation of the MDM4/2-p53-IGF-1 pathway has been shown to be critical for axonal sprouting and neurological recovery after spinal cord injury.[27] OPN is a secreted phosphoprotein that binds to receptors recognizing the Arg−Gly−Asp protein motif.[28] OPN is implicated in maintenance and reconfiguration of tissue integrity during inflammation by modulating the extracellular matrix (ECM).[29] In a stroke model in Sprague−Dawley rat, OPN has been shown to be neuroprotective,[30] and in combination with IGF-1, OPN has been shown to promote regeneration of alpha RGCs after axotomy.[31] Phosphatase tension homologue (PTEN) is a phosphatase that dephosphorylates PIP_3 to PIP_2 resulting in inhibition of the Akt/mTOR pathway. PTEN deletion by virus mediated gene silencing has been shown to prevent RGC apoptosis after ON cut[32] and enhance the regenerative potential of neurons in the corticospinal tract.[33]

For clinical translation, combining mTOR pathway stimulating biologics for RGC neuroprotection requires modifications that would provide better control over cell pathway modulator (*i.e.*, promoters, inhibitors, inducers, agonists and antagonists) delivery, release, clearance and residency time. Nanocarriers represent one of many possible solutions (*e.g.*, microcarriers, implants, *etc.*) in delivering multiple cell pathway modulators while controlling modulator release. Nanocarriers protect sensitive cargos from degradation, can reduce the effect of clearance mechanisms and improve absorption of cargos across physiological barriers. Liposomes, phospholipid vesicles frequently containing cholesterol, are an attractive delivery system for retina diseases,[34] offering loading of both hydrophobic and hydrophilic molecules, prolonged retention in the eye after intraocular (intravitreal or subretinal) injection,[35−39] protection of cargo from degradation[40] and have a history of clinical approval.[41] The majority of liposomal research in central nervous system (CNS) aspects is associated with overcoming the blood brain barrier to improve the delivery of drugs to the brain.[42−44] Liposomes and lipoplexes have been shown to effectively deliver the RPE65 gene, critical for vision, in RPE65 knockout blind mice leading to an improvement in vision.[39] Limited work has been reported on neuroprotection and nerve regeneration. Cationic liposomes and corresponding lipoplexes have been used to transfer neurotrophic factor genes (e.g., glial derived neurotrophic factor, nerve growth factor *etc.*) in both spinal cord and brain injury models.[45,46] These studies have shown neuroprotection and partial restoration of locomotor function.[45,46] Immunomodulation, via the selective apoptosis of monocytes and phagocytic macrophages using clodronate loaded liposomes, has shown partial hindlimb recovery and neuron repair in a rat spinal cord injury model.[47] To our knowledge, liposomes loaded with multiple cell pathway have not previously been reported for CNS neuroprotection and regeneration. Liposomes loaded with multiple cell pathway modulators have the advantage of delivering theses modulators to the cell microenvironment at the same time, facilitating a synergistic effect on single or multiple cell pathways. Furthermore, signaling pathway modulators are often highly efficacious and only very low concentrations are required. This reduces the need for high drug loading and maximizing the space available to pack a range of therapeutic small molecules, peptides and proteins into the liposome.

In this study, we present two liposome formulations that promote neuroprotection through stimulating the mTOR pathway. Liposome aqueous cores were loaded with CNTF and IGF-1. Liposome membranes were loaded with lipid conjugated peptides OPP and either PAP2 or PAP4. OPP is a peptide analogue of the N-fragment of OPN (specifically the RGD and $\alpha_9\beta_1/\alpha_4\beta_1$ domains[29]) that has been shown to mimic the function of recombinant human OPN[48] and lower cytosolic Ca^{2+} in a way similar to OPN.[49] PAPs are PTEN antagonist peptides with PAP2 targeting the ATP B type domain and PAP4 targeting the c-terminal tail of PTEN.[50] We show that multifarious mTOR pathway stimulating biologic loaded liposomes significantly prevent RGC death and loss of retina electrophysiological function in a *N*-methyl-D-aspartic acid (NMDA) mouse model. To further explore combination therapy, we combine one neuroprotective liposome formulation with induced pluripotent stem cell (iPSC) derived RGC transplantation in the NMDA mouse model and show improved electrophysiological outcome of the transplantation.

RESULTS AND DISCUSSION

Liposomes. The palmitoyl (C_{16}) conjugated peptides (*i.e.*, lipopeptides) C_{16}-OPP, C_{16}-PAP2, and C_{16}-PAP4 (referred to as OPP, PAP2, and PAP4 from now on), were all successfully synthesized and purified by semipreparative reverse phase HPLC to a purity of >95% confirmed by HPLC and MALDI-TOF MS (Supplementary Figures S1 and S2). Liposomes were produced as illustrated in Figure 1A. Liposomes showed low polydispersity index (PDI < 0.1) with diameters close to 100 nm in both DLS measurements (Figure 1B) and cryoTEM images (Figure 1C). CryoTEM images showed spherical liposomes that were predominantly unilamellar. All liposomes had a negative zeta potential, which is important for reducing cytotoxicity[51,52] and in combination with surface PEGylation has been shown to improve liposome diffusion throughout the vitreous.[53] Lip A and Lip B showed a slightly more negative zeta potential than Lip C (−19 mv, −18 mv, and −13 mV, respectively). The zeta potential of all the liposomes is similar to previously reported values of unilamellar liposomes with similar phospholipid compositions.[54−56]

The encapsulation efficacy (EE%) normalized to the lipid concentration was higher for Lip B than the EE% of Lip A, and both formulations showed a higher EE% of CNTF (~22 kDa) than IGF-1 (7.7 kDa). These EE% approximately corresponded to 700 nM IGF-1 and 763 nM CNTF concentrations for Lip A, while for Lip B the concentrations were 1.53 μM IGF-1 and 1.27 μM CNTF. These values indicate that IGF-1 and CNTF both loaded in approximately a 1:1 ratio in both formulations and that macromolecule size did not influence loading. These concentrations were well above the IC50 values of IGF-1 and CNTF (*i.e.*, < 6 nM),[57,58] while keeping the injected concentration of CNTF low enough to not induce suppression of retina electrophysiological function.[59]

The difference in EE% between the two formulations is likely to be due to the different PTEN inhibitor lipopeptides

DOI: 10.1021/acsnano.8b00596
ACS Nano 2018, 12, 7497−7508

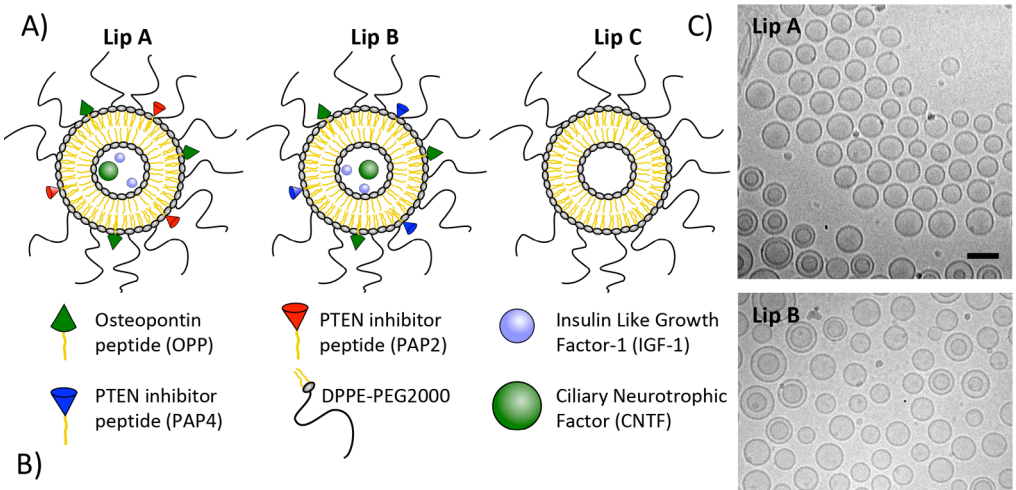

B)

Liposome	Lip A	Lip B	Lip C
Diameter (nm)	108.7±1.8	96.9±6.1	99.0±10.8
PDI (AU)	0.04±0.02	0.06±0.01	0.05±0.01
Zeta potential (mV)	-19.2±1.4	-18.0±2.1	-12.8±1.3
EE% IGF-1	2.1±1.1	4.6±2.6	-
EE% CNTF	6.6±4.5	11.7±2.9	-

Figure 1. Liposome characterization: (A) Schematic drawing of liposomes with encapsulated IGF-1, CNTF, lipopeptide OPP, and lipopeptide PTEN inhibitors (PAP2 or PAP4); (B) liposome size, polydispersity index (PDI), zeta potential, and protein encapsulation efficiency. Liposome diameter and PDI were measured by DLS in HBS, zeta potential was measured in 10 mM HEPES with 5% glucose. Encapsulation efficiency (EE%) of spin-filter purified liposomes was assessed by ELISA (N = 3); (C) CryoTEM images of liposome formulations (scale bar = 100 nm).

incorporated into the membrane. PAP2 has a cysteine with a free thiol group that can react with other thiol groups, either from other PAP2 lipopeptides in a liposome bilayer or on proteins (*e.g.*, present in FBS, IGF-1, *etc.*), possibly reducing protein loading or increasing liposome leakiness during purification. This is supported by the observation that neither Lip A or Lip B leaked calcein (a small hydrophilic fluorescent dye) at 37 °C in HBS. However, Lip A did leak calcein over time when 10% FBS was added to HBS at 37 °C (Supplementary Figure S3), indicating an interaction that resulted in liposome bilayer instability. The low EE% ensured that the proteins were fully hydrated and did not aggregate inside the liposomes. This is supported by the absence of visible internal structures in the cryoTEM images in Figure 1C. The bioactivity of Lip A and Lip B was tested *in vitro* in HEK293T cells (Supplementary Figure S4). Phosphorylation of Akt and p70S6K was observed for both formulations, indicating that the cargos remained biologically active.

Liposome Uptake in Retinal Organoids. The cellular uptake of liposomes was tested *in vitro* in retinal cell organoids differentiated from mouse embryonic stem (mES) cells (Figure 2A).[60] This system has advantages over traditional 2D cultures, including more relevant pharmacokinetic results.[61−63] Retinal organoids were cultured for 21 days and then exposed to liposomes labeled with Atto655 for 12 h. The level and cell specificity of uptake was quantified by flow cytometry (Supplementary Figure S5). The overall uptake of liposomes (Figure 2A) showed that Lip B had the lowest uptake with approximately 13% of cells showing uptake. The control liposome, Lip C, showed a slightly higher cellular uptake (18% of cells) than Lip B. The highest uptake was observed for Lip A with 23% of cells showing uptake. The variance between replicas of Lip A was significantly larger than that of either Lip B or Lip C. Statistical analysis between the liposome formulations was carried out, and none of the formulations showed significantly different uptake compared to Lip C. However, Lip A had a significantly higher uptake than Lip B. The higher uptake observed for Lip A might be explained by sulfur−sulfur interactions between the cysteine in PAP2 and thiol groups on the cell surface. Cell surface thiols interacting with thiols present on nanomaterials has been argued as a mechanism to enhance uptake into cells.[64]

Retinal organoids were approximately 1 mm in diameter (Figure 2A). Retinal cells are between 9 and 12 μm in diameter[65] and assuming organoids are densely packed perfect spheres then approximately 1% of the cells are located on the organoid surface, indicating that the liposomes were capable of moving (*i.e.*, by active transport and/or passive diffusion) beyond the surface layer of cells. It has previously been reported that nanocarriers can penetrate beyond the surface layer of cells in 3D cell aggregates.[66−68] To determine if liposome uptake was associated with specific cell types, organoids were dissociated and stained for five major retinal cell type markers. The markers used were antirecoverin-Rb-IgG (Chemicon) for photoreceptor cells,

DOI: 10.1021/acsnano.8b00596
ACS Nano 2018, 12, 7497−7508

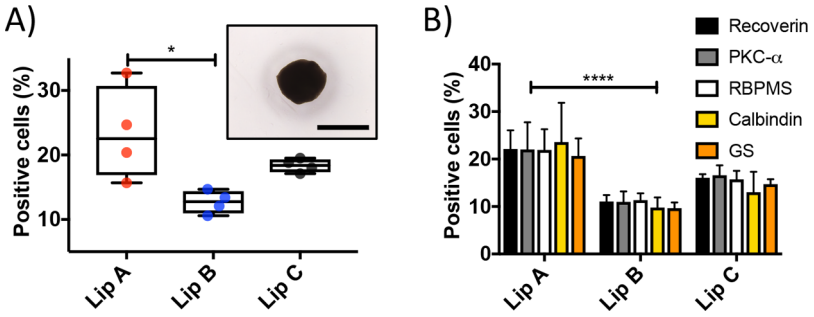

Figure 2. Liposome uptake in retinal organoids. (A) Box and whiskers plot of the total liposome uptake (as % positive cells for Atto655) in retinal organoids (*$P \leq 0.05$ between Lip A and Lip B, $N = 4$). Inset shows an example micrograph of a retinal organoid cultured to day 21 (scale bar, 1 mm). The box plot median values are 22.6%, 12.8%, and 18.4% for Lip A, Lip B, and Lip C, respectively. (B) Liposome uptake (as % positive cells for Atto655) in specific cell types found in retinal organoids using cell markers. The cell types shown are photoreceptors (recoverin), bipolar cells (PKC-α), RGCs (RBPMS), horizontal cells (calbindin), and Müller glia cells (glutamine synthetase (GS)). Error bars show standard error of the mean (**$P \leq 0.0001$ between Lip A and Lip B, no significant difference between cell types, $N = 4$).**

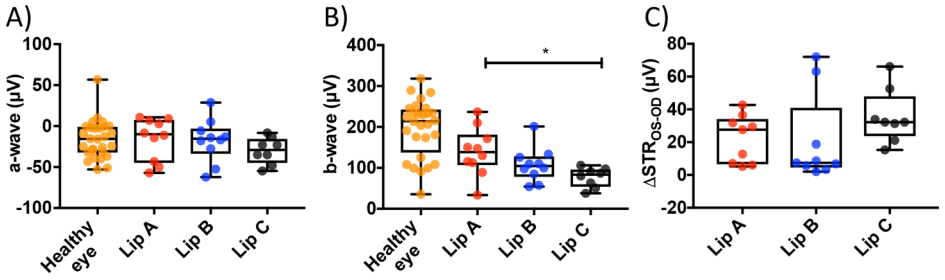

Figure 3. Electroretinogram amplitude values from dark-adapted mice. (A) A-wave response for healthy and treated eyes. Box plot median values are −15.6 μV for healthy eye, −9.9 μV for Lip A, −15.5 μV for Lip B, and −29.1 μV for Lip C. (B) B-wave response for healthy and treated eyes (*$P \leq 0.05$ between Lip A and Lip C). Box plot median values are 214.3 μV for healthy eye, 138.7 μV for Lip A, 104.7 μV for Lip B, and 83.5 μV for Lip C. (C) The change in scotopic threshold response, ΔSTR (pSTR − nSTR), between the healthy left (oculus sinister, OS) and liposome treated damaged right (oculus dexter, OD) eyes. Box plot median values are 27.6 μV for Lip A, 7.4 μV for Lip B, and 32.2 μV for Lip C. Highly negative values (greater than −10 μV) were excluded from ΔSTR assuming natural visual impairment in the healthy control eye. $N = 8–10$ mice per liposome treated group, $N = 28$ mice for healthy control eye.

anti-PKC-α-m-IgG (Santa Cruz) for bipolar cells, anti-RBPMS-Rb-IgG (Abcam) for RGCs, anticalbindin-Rb-IgG (Sigma-Aldrich) for horizontal cells and antiglutamine synthetase-Rb-IgG (GS) (Abcam) for Müller glia cells.[69,70] No difference in uptake between the different cell types was observed (see Figure 2B) but it should be noted that retinal cells are not fully mature at day 21.

***In Vivo* Preservation of Retinal Function by Loaded Liposomes.** RGC death was induced in the right eye of C57BL/6J mice by a single intravitreal injection of *N*-methyl-D-aspartic acid (NMDA, 2 μL at 20 mM). Mice were divided into three treatment groups receiving 1 intravitreal injection of either Lip A, Lip B, or Lip C liposomes 2 h after the NMDA injection. Four weeks after the liposome treatment the retinal function of dark-adapted mice were evaluated by electroretinography (ERG) and eyes were enucleated for histological analysis (Supplementary Figure S6). NMDA treated mice receiving empty liposomes (Lip C) were used as controls. NMDA binds irreversibly to the NMDA receptor at the postsynaptic membrane leading to an excessive influx of positive ions (*e.g.*, Ca^{2+}), depolarizing the mitochondrial membrane and ultimately triggering apoptosis.[71−73] NMDA has shown retinal toxicity at low concentrations (*e.g.*, 20 nM) with the degree of inner retina damage corresponding to NMDA concentration.[74] NMDA affects other retina cell types and intravitreal administered NMDA also induces partial optic nerve damage, likely linked to the damage of the inner retina. A 20 mM NMDA injection is an extreme model of retina damage. We observed no significant difference in a-wave response (Figure 3A), associated with photoreceptors, between healthy control eyes and NMDA-injected eyes. This confirmed that intravitreal NMDA injection at 20 mM concentration did not result in photoreceptor damage, which is consistent with previous observations.[74,75]

The b-wave response, associated with the function of interneuron cells (*e.g.*, amacrine and horizontal) and bipolar neuron cells,[72,76,77] showed a significant decrease in all NMDA-injected groups (Figure 3B) compared to healthy controls. At low concentrations (<50 nM) NMDA has been shown to damage amacrine cells but bipolar cell damage has only been reported for higher concentrations (>200 nM).[78] At 20 mM NMDA concentrations, substantial bipolar and interneuron cell damage will have occurred. We observed a significant protective effect of Lip A compared to the empty liposome Lip C (P value < 0.02). Lip B showed no significant difference in b-wave response compared to either the Lip A or Lip C treated groups. The Lip B treated group did show a trend which indicated a minor preservation of b-wave response than the Lip C treated group. A-wave and b-wave amplitudes in healthy eyes between C57BL/6J mice were similar to previous reports.[79]

Scotopic threshold response (STR, Figure 3C) has been related to the function of the inner retinal neurons more proximal than the bipolar cells (*e.g.*, RGCs).[2,75,80,81] To estimate the neuroprotective effect, the difference in STR amplitudes (pSTR − nSTR) between the healthy (left) and treated (right) eye for each animal was determined (*i.e.*, $\Delta STR_{OS\text{-}OD}$, Figure 3C). A lower $\Delta STR_{OS\text{-}OD}$ therefore means a return of function and

DOI: 10.1021/acsnano.8b00596
ACS Nano 2018, 12, 7497−7508

an inner retinal neuronal response closer to the healthy eye, with full restoration giving a $\Delta STR_{OS\text{-}OD} = 0$. For $\Delta STR_{OS\text{-}OD}$, no significant difference was found between the treatment groups (ANOVA $p > 0.05$). However, both Lip A and Lip B treated groups showed clear trends toward better preservation of STR. For Lip A the spread of data points is divided into two groups suggesting a bimodal distribution (responsive and unresponsive), in which the responsive group has a $\Delta STR_{OS\text{-}OD}$ of ~7 μV. The Lip B treated group showed a more unimodal distribution with more than 75% of the mice around the median $\Delta STR_{OS\text{-}OD}$ of 7.4 μV (the median for Lip C treated group is 32.2 μV for comparison).

Extrapolation of the ERG data would indicate that Lip A had a significant protective effect on interneuron and bipolar neuron cells but a mixed effect on RGCs. Conversely, Lip B showed no significant protective effect on interneuron and bipolar cells but indicated a protective effect on RGCs. The reasons for this observation are likely manifold. PTEN inhibition may be a critical factor and peptides that inhibit regions of PTEN might induce different responses in different cell types. Equally, the concentrations of IGF-1 and CNTF needed for protection combined with appropriate release kinetics might be specific to specific cell types. Interestingly, NMDA activation of the p38 MAPK pathway has been shown to be pro-apoptotic for RGCs and pro-survival for photoreceptors.[82] Given IGF-1 and CNTF will promote a number of signaling pathways (e.g., MAPK for IGF-1) and that signaling pathway dynamics are likely different between specific cell types, loading multiple pathway regulators into liposomes may lead to specific effects (positive and negative) on specific cell types rather than promote positive effects in tissue as a whole.

***In Vivo* Rescue of RGCs by Loaded Liposomes.** To evaluate the effect of a single intravitreal injection of Lip A and Lip B on host RGC survival after NMDA induced RGC death, retinal whole mounts were stained for RBPMS and imaged on a confocal microscope. Three images per retina were acquired, approximately 1 mm away from the optic nerve head. Example micrographs from a healthy control eye, an eye threated with Lip A, and an eye treated with Lip C are shown in Figure 4 panels A, B, and C, respectively. RGCs in each image were counted and the average number of surviving RGCs in the three images was calculated to enable quantitative comparison between the groups (Figure 4D). NMDA injection in combination with Lip C resulted in substantial RGC loss (~75% loss compared to the healthy controls). This observation is consistent with previous quantifications of RGC loss in mice without empty liposomes.[83] This result showed that Lip C did not have a neuroprotective effect. Treatment with either Lip A or Lip B was not able to completely prevent RGC loss.

Statistical analysis showed a significant difference between Lip A and Lip C treated groups but no difference between Lip B and Lip C treated groups (552 cells/mm^2, 379 cells/mm^2 and 360 cells/mm^2 median values for Lip A, Lip B and Lip C respectively). The RGC rescue data indicated that although Lip B showed a trend to preserve the electrophysiological function associated with RGCs, this did not translate into a greater number of rescued RGCs. Lip A treated mice showed the greatest variance in surviving RGCs and also showed a bimodal trend in STR. This indicates that a number of mice within the group responded very well to the treatment with Lip A, probably due to a range of reasons. There is a lack of knowledge in the supportive role, if any, of amacrine and bipolar cells on RGC survival. Given Lip A improved b-wave response

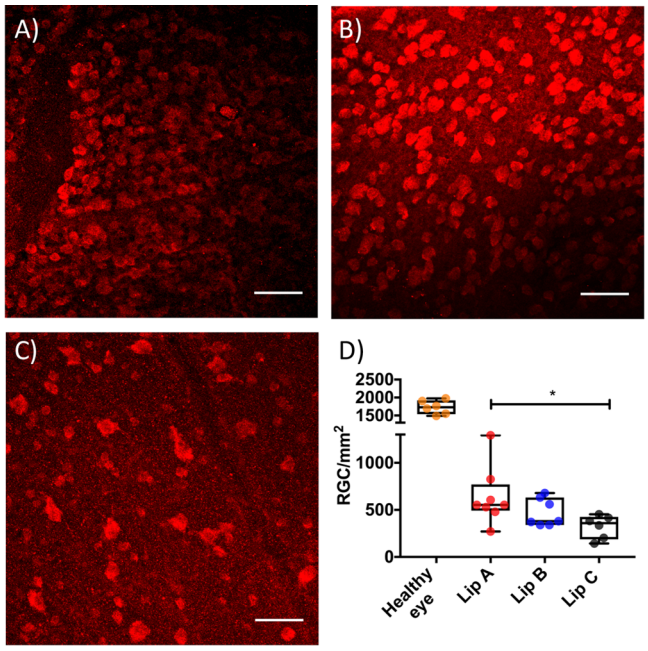

Figure 4. RGC rescue by liposomes after NMDA induced damage of mouse retinas. Example retina micrographs from (A) a healthy control eye; (B) a Lip A treated eye, and (C) a Lip C treated eye. In all micrographs RGCs nuclei were labeled with RBPMS Alexa647 (red), white scale bars are 60 μm. (D) Box and whiskers plot showing the density of surviving RGCs in healthy and liposome treated damaged eyes (*$P \leq 0.05$ between Lip A and Lip C). Each dot shows an average RGC density for an eye, calculated from three micrographs taken 1 mm away from the optic nerve head. The box plot median values are 1728 RGCs/mm^2 for the healthy eye, 553 RGCs/mm^2 for Lip A, 380 RGCs/mm^2 for Lip B, and 360 RGCs/mm^2 for Lip C. $N = 6–8$ mice per group.

(associated with amacrine and bipolar cells) and showed the greatest number of surviving RGCs it would indicate that amacrine and bipolar cells support RGC survival. However, the STR for Lip A treated mice indicates that although there are more RGCs present than in Lip B treated mice, the function of these RGCs has been compromised.

Loaded Liposomes in Combination with Transplant RGCs Improve $\Delta STR_{OS\text{-}OD}$. We investigated the effect of the liposomes in combination with RGC transplantation. NMDA and liposome injections were performed as described above. Transplant RGCs (tRGCs), differentiated from Thy1-GFP induced pluripotent cells (iPSC)[84] were transplanted by intravitreal injection 4 days after NMDA injection. Retina progenitor cells and neuroretinal cells have both been proposed as cell therapies and cell transplants into both young animals and *ex vivo* retinas have shown some success.[85,86] However, good integration and survival of transplant cells in adults remain a challenge.[87] The combinatorial effect of liposomes and RGC transplantation was evaluated by retina electrophysiological function and donor cell survival 4 weeks after the transplantation (Figures 5 and 6). We chose Lip A as the liposome formulation due to improved RGC survival, better b-wave response, and the indication that STR was preserved in approximately 50% of mice.

No difference in a-wave response was observed between the healthy eyes and the treated eyes (Figure 5A). The b-wave response showed a significant difference between the treated groups and healthy control as well as between the two treated

DOI: 10.1021/acsnano.8b00596
ACS Nano 2018, 12, 7497–7508

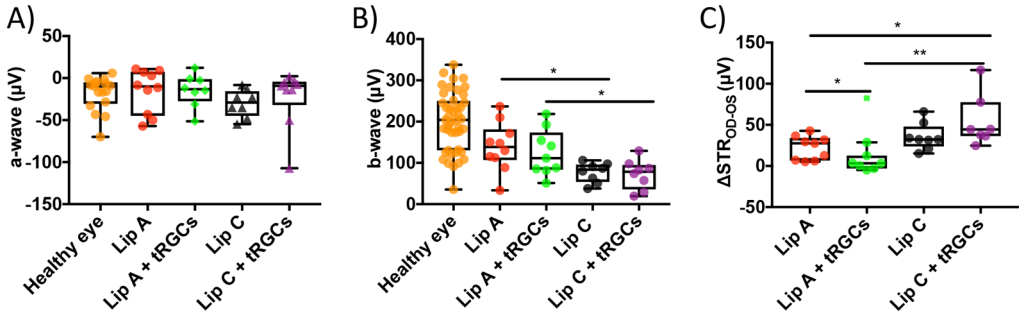

Figure 5. Electroretinogram amplitude values from dark-adapted mice undergoing treatment with liposomes and transplant RGCs (tRGCs). (A) A-wave response for healthy and treated eyes. (B) B-wave response for healthy and treated eyes (*$P \leq 0.05$ between Lip A + tRGCs and Lip C + tRGCs. *$P \leq 0.05$ between Lip A and Lip C). (C) $\Delta STR_{OS\text{-}OD}$ for liposome treated and liposome plus tRGC treated damaged eyes compared to healthy controls. Highly negative values (greater than −10 μV) were excluded from the ΔSTR assuming natural visual impairment in the control eye. One outlier was identified in the Lip A + tRGCs group and excluded from the statistical analysis (*$P \leq 0.05$ between Lip A and Lip A + tRGCs. *$P \leq 0.05$ between Lip A and Lip C + tRGCs. **$P \leq 0.01$ between Lip A + tRGCs and Lip C + tRGCs). N = 8−10 mice per treated group, N = 17−44 mice for healthy control (panels A and B). N = 7−9 mice per treated group (panel C).

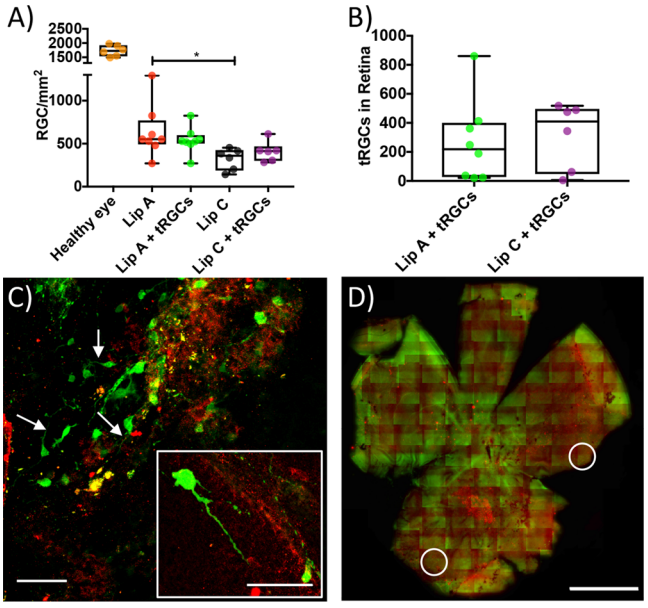

Figure 6. Host and transplant RGC survival. (A) Box and whiskers plot showing host RGC density in healthy eyes (median = 1728 cells/mm^2) and NMDA damaged host eyes (median values for Lip A + tRGCs = 528 RGCs/mm^2, Lip C = 360 RGCs/mm^2, and Lip C + tRGCs = 415 RGCs/mm^2) 4 weeks after NMDA injection (*$P \leq 0.05$ between Lip A and Lip C). (B) Box and whiskers plot of tRGC survival in combination with liposomes (median values of 219 and 409 for Lip A and Lip C, respectively). (C) Example micrographs from the Lip A + tRGCs group. Transplant RGCs are in green, host RGCs in red (white arrows indicate axons, scale bar = 60 μm). The insert figure shows an example tRGC with axon (scale bar = 60 μm). (D) Example whole retina tile scan from the Lip A + tRGCs group used for cell counting. In all microscopy images tRGCs are in green (GFP) and host RGCs are in red (RBPMS). White circles highlight example areas containing tRGCs (scale bar = 1 mm, see Supplementary Figure S9 for larger image). N = 6−8 mice per group (panels A and B).

groups (Figure 5B). There was no significant difference in b-wave response between Lip A treated and Lip A in combination with tRGCs treated mice. This result indicated that the transplant RGCs (tRGCs) did not contribute to the b-wave response and that Lip A alone had a protective effect. This is corroborated with the b-wave response for tRGCs combined with Lip C, which resulted in similar b-wave amplitudes to empty liposomes (*i.e.*, Lip C) alone. The $\Delta STR_{OS\text{-}OD}$ data (Figure 5C) showed that a combination of Lip A and tRGCs resulted in a significant rescue of RGC associated electrophysiological function (median = 3.3 μV) compared to Lip A treatment alone (median = 27.6 μV). Lip C in combination with tRGCs showed no rescue of STR, while Lip A in combination with tRGCs resulted in a significant improvement in $\Delta STR_{OS\text{-}OD}$ compared to all other treatments. The ERG data does indicate that the loaded liposomes (Lip A) support tRGCs in a manner that improved host STR. The observation that empty liposomes (Lip C) in combination with tRGCs showed no rescue of STR supports this argument. Interestingly, Lip A in combination with tRGCs significantly reduced $\Delta STR_{OS\text{-}OD}$ variance and eliminated the bimodal distribution seen in Lip A alone. These results indicate that both activation of cell growth signal pathways and the protection of other retina cell types (*e.g.*, amacrine, bipolar, *etc.*) may be critical to transplant RGCs restoring host tissue function.

The effect of the combined treatment on host RGCs survival was evaluated by RBPMS staining and confocal microscopy (Figure 6). The host RGC density of the healthy control eyes and the treated eyes are shown in Figure 6A. We were not able to identify a significant additive effect of tRGCs on host RGC survival (552 cells/mm^2 for Lip A and 527 cells/mm^2 for Lip A + tRGCs). This indicated that it was Lip A alone that promoted host RGC survival. Next, we investigated the effect of the liposomes on the survival of tRGCs. Retinal whole mounts were double-stained for GFP (marker for tRGCs) and RBPMS (host and transplant RGCs). Host RGCs expressed RBPMS at higher levels than the tRGCs resulting in limited colocalization of red and green fluorescence for the tRGCs. It is worth emphasizing that the low RBPMS expression in tRGCs is likely due to the tRGCs not yet being fully mature (Supplementary Figure S7). tRGC survival was observed in both Lip A and Lip C groups (Figure 6 and Supplementary Figure S8) 4 weeks after transplantation, showing a longer survival time for tRGCs compared to previous reports on transplanted cells.[88−90]

Axon sprouting was observed in both Lip A and Lip C groups when combined with tRGCs (Figure 6C). Surviving tRGC numbers after 1 month were very low and no significant difference in survival of the transplanted cells was observed between Lip A and Lip C groups. Transplant cell survival is a major challenge in cell transplantation.[87] Additionally, the NMDA induced apoptotic environment in the host eye will

DOI: 10.1021/acsnano.8b00596
ACS Nano 2018, 12, 7497−7508

have also induced tRGC apoptosis as NMDA induced toxic effects to retina cells has been shown to have a prolonged duration (up to 14 days).[74] The nonspecific (*i.e.*, not associated with intact cells) green fluorescence observed in the whole retina tile scans is likely GFP debris from the tRGCs combined with tissue autofluorescence (Figure 6D). Transplant cell survival has been shown to be improved by injury and loss of host RGCs.[91] The rescue of host RGCs by Lip A may explain the lack of an observed effect of Lip A on tRGC survival. Another possible explanation could be linked to the timing and concentration of the delivered mTOR pathway promoters. Delivery of growth factors at appropriate concentrations is important for RGC survival in the neonatal retina and likely to be critically important in inducing a significant positive effect on the survival of transplanted cells.

CONCLUSION

Liposomes loaded with multiple mTOR pathway stimulating biologics showed a significant improvement in retina electrophysiological function after a single injection in an NMDA mouse model with extensive retina damage. Multifarious mTOR pathway stimulating biologic loaded liposomes improved b-wave response and STR. These liposomes also improved host RGC survival after NMDA exposure. Liposomes in combination with tRGCs showed a significant improvement in STR compared to liposomes alone. This indicated that liposomes improved the electrophysiological outcome of the transplantation. The results show that multifarious mTOR pathway stimulating biologic loaded liposomes can facilitate both neuroprotection across a number of specific cell types and RGC transplantation. Further research, particularly in dosing dynamics (*e.g.*, modulator concentrations, modulator combinations, number of injections, time between injections, *etc.*), is required to develop clinically viable neuroprotective and transplant facilitating nanomedicines.

METHODS

Lipopeptide Synthesis. All peptides were synthesized using a Biotage Initiator Alstra peptide synthesizer (Biotage) on a TentaGel S RAM resin (Sigma-Aldrich) at the 0.5 mmol scale using established solid phase methods (Supplementary Figure S1).[92] All chemicals (*e.g.*, amino acids, solvents, coupling agents, *etc.*) were purchased from Sigma-Aldrich or Bachem. Briefly, couplings were 5 min at 75 °C using 4 equiv amino acid, 3.92 equiv *O*-(7-azabenzotriazol-1-yl)-1,1,3,3-tetramethyluronium hexafluorophosphate (HATU), and 8 equiv 2,4,6-collidine in DMF. Fmoc deprotection was done using 20% piperidine in DMF. Peptides were conjugated to palmitic acid (C_{16}) at the N-terminus using established HATU/collidine coupling chemistry (1:2:4 molar ratio for palmitic acid/HATU/collidine) to form lipopetides and cleaved from the support using trifluoroacetic acid, water, and triisopropylsilane (95:2.5:2.5). In the case of PAP2 cleavage was performed using trifluoroacetic acid, water, triisopropylsilane and ethanedithiol (92.5:2.5:2.5:2.5).

Lipopeptides were precipitated in cold diethyl ether and filtered off. Crude lipopeptide was dissolved in a acetonitrile:water (1:1) solution and purified using preparatory HPLC (Waters) on a C18 column (Xterra). A water (5% acetonitrile, 1% trifluoroacetic acid) acetonitrile (0.1% trifluoroacetic acid) gradient was used starting at 10% acetonitrile and increasing to 60% acetonitrile over 25 min. All lipopeptides had a purity ≥95%. Lipopeptide molecular weight was confirmed using a autoflex MALDI-ToF MS (DHB, 0.1% TFA matrix, Bruker) and purity by analytical HPLC (C8 column, Gilson). The lipopeptides had the following sequences: (OPP) C_{16}-PTVDVPDGRGDSLAYGLRSK; (PAP2) C_{16}-KHKNHYKIYNLCAE; and (PAP4) C_{16}-TVEEPSNPEASSSTSVTPD. Lipopeptide HPLC chromatograms and MALDI-ToF MS spectra can be found in the Supporting Information (Supplementary Figure S2).

Preparation of Liposomes and Loading of Proteins. All lipids were purchased from Avanti Polar Lipids and had a purity of ≥98%. Liposomes were prepared by dissolving pure lipids in 9:1 tertiary butanol/water and then pipetting them together to give the relevant lipid mixtures. The lipid mixtures were then lyophilized to dry lipid powders overnight using freeze-drying. The lipid powders were subsequently hydrated over 1 h by adding 10 mM HEPES buffered saline pH = 7.4 (HBS) at 60 °C and shaking every 10 min. The liposomes were extruded through a 100 nm pore size filter 21 times at 60 °C and stored at 4 °C until use. Liposomes were composed of 1,2-dipalmetoyl-*sn*-glycerol-3-phosphatidylcoline (DPPC), cholesterol (Chol), 1,2-dipalmitoyl-*sn*-glycero-3-phosphoethanolamine-*N*-[methoxy-(polyethylene glycol)-2000] ammonium salt (DPPE-PEG2000), OPP, and PAP2 or PAP4. Liposome A (Lip A) comprised DPPC/Chol/DPPE-PEG2000/OPP and PAP2 in a 53:40:5:1:1 mol % ratio. In liposome B (Lip B), PAP2 was replaced with PAP4 at the same mol %, all other lipid percentages were the same. A control liposome (Lip C) without any proteins or lipopeptides had a composition of DPPC/Chol/DPPE-PEG2000 (55:40:5 mol %).

The proteins were loaded into preformed liposomes following established methods.[93] Briefly, CNTF and IGF-1 (recombinant human CNTF and recombinant human IGF-1, Cell Guidance Systems) were dissolved in HBS at 0.25 mg/mL and mixed with liposomes. The mixture was snap frozen in liquid N_2 and thawed in a water bath at 37 °C, this process was repeated once. Nonencapsulated proteins were removed by spin-filtration with a 100 kDa spin filter (Merck), using HBS as eluent. The concentration of encapsulated protein was determined by ELISA (R&D Systems) following the instructions of the manufacturer. Lipid concentrations were detected by ICP-MS (Thermo Scientific). Encapsulation efficiency (EE%) of the CNTF and IGF-1 was determined by normalizing the protein concentration before and after purification to the actual lipid concentration, as described in eq 1.

$$\mathrm{EE\%} = \frac{[\mathrm{protein}]_{\mathrm{end}}/[\mathrm{lipid}]_{\mathrm{end}}}{[\mathrm{protein}]_{\mathrm{start}}/[\mathrm{lipid}]_{\mathrm{start}}}100 \quad (1)$$

.Normalizing protein concentration to lipid concentration, rather than describing EE% as a change in protein concentration only, takes into account changes in volume from purification steps.

Liposome Characterization by DLS and Zeta-Potential. Liposome hydrodynamic diameter and zeta-potential were measured on a Brookhaven ZetaPALS. For size measurements liposomes were diluted in HBS. Zeta-potential was measured on liposomes diluted in 10 mM HEPES, 5% glucose at pH 7.4.

***In Vitro* Liposome Stability.** Liposome stability was evaluated at 4 °C by following changes in size and polydispersity index (PDI) of loaded liposomes over time. Sizes and PDI were measured by DLS as described above. The ability of the liposomes to retain the loaded content was assessed by encapsulation of a self-quenching concentration (20 mM) of the hydrophilic fluorophore, calcein (Sigma-Aldrich). Liposomes were formulated as described above, adding 20 mM calcein in HBS for hydration of the lipid powder. Nonencapsulated calcein was removed by size exclusion chromatography (SEC) on a Sephadex G50 column using HBS. The calcein loaded liposomes were then split into different vials, kept at 4 or 37 °C. A 100 μL aliquot of each sample at a concentration of 0.1 mM was subsequently transferred to a black flat bottom 96 well plate, and the fluorescent signal was measured in a plate reader (Wallac Victor^3 1420 Multilabel Counter) before and after lysing the liposomes with 2 μL of 10% Triton X (Sigma-Aldrich). The ratio of the fluorescent signal of lysed liposomes over intact liposomes was then plotted against time to generate a leakage profile.

Bioactivity assay of liposomes by Western Bolt. To test the ability of Lip A and Lip B to influence the mTOR/Akt pathway, HEK293T (Sigma-Aldrich) cultured in Dulbecco's modified eagle's medium (DMEM) supplemented with 10% fetal bovine serum (FBS) (Sigma) and 5% penicillin–streptomycin in a six well plate was

DOI: 10.1021/acsnano.8b00596
ACS Nano 2018, 12, 7497–7508

incubated for 12 h with 0.4 mM liposomes at 37 °C 5% CO_2. Cells incubated with Lip C were used as a control. Semiquantitative analysis for Akt activation was performed by Western blot (WB) following standard protocol. In brief, cells were washed with cold PBS and collected by mechanical scraping in 200 μL of cold PBS, with phosphatase inhibitor cocktail 2 (Sigma-Aldrich) and complete Mini EDTA free protease inhibitor cocktail (Roche). Cells were transferred to clean 1.5 mL tubes kept on ice. The cells were lysed by adding 200 μL of hot (∼96 °C) 4× protein loading buffer (Li-Cor) with 10% mercaptoethanol (Sigma-Aldrich), and the mixture was boiled for 5 min before loading 15 μL of the whole cell lysate in a 1.5 mm Nu PAGE 4−12% Bis-Tris Gel (Invitrogen). Five microliters of chameleon 700 prestained protein ladder (Li-Cor) was loaded in the outermost wells. Electrophoresis was run at 100 V in Nu PAGE running buffer (Invitrogen) for 2 h.

The proteins were transferred to a nitrocellulose membrane (Invitrogen) in 25 mM Tris, 190 mM glycine, and 20% methanol buffer at pH 8.3. The nitrocellulose membrane was blocked with odyssey blocking buffer for 1 h at room temperature, washed with Tris buffered saline (Sigma-Aldrich) 0.1% Tween 20 (Sigma-Aldrich) (TBST), and stained with anti-Akt1-Rb-IgG (abcam) overnight at 4 °C. The membrane was washed with TBST and incubated for 1 h with secondary stain Gt-anti-Rabbit IgG DyLight 800 (Invitrogen) before imaging the membrane on an Odyssey FC imaging system (Li-Cor). The antibody was then stripped using Revitablot Western blot stripping buffer (Rockland) before reblocking, and staining overnight with anti-Akt1/2/3-Rb-IgG (Abcam) at 4 °C. Akt1/2/3 was labeled with IRDye 680RD Gt-anti-Rb (Li-Cor) and imaged. The same methodology was used for p70S6 kinase, except anti-p70S6K-Rb-IgG (Invitrogen), and anti-Phospho-p70S6K (Thr421, Ser424)-Rb-IgG (Invitrogen) were used. Densitometry was made by drawing rectangles over appropriate bands, obtaining the intensity, and dividing the intensity by the control (*e.g.*, Akt1/2/3 or p70S6K).

Culture of Retinal Organoids. Murine embryonic stem cells (mESCs) were thawed and seeded in T75 flasks precoated with 1% Matrigel in DMEM for 20 min. Cells were cultured in ESC maintenance medium (ES medium, see Supporting Information for all media components), at 37 °C, 5% O_2, 5% CO_2, until 80% confluency. Cells were then collected by trypsinization and seeded in 96 tissue culture plates (Falcon Corning) at 20 000 cells/well in optic vesicle media (OV-medium) (Day 1). After seeding on day 2, 1% Matrigel in 50 μL of OV medium was added to each well. At day 5, 100 μL of 0.5% Matrigel in OV medium was added. Day 9, 100 μL of media from each well was replaced with 100 μL of optic cup medium (OC-medium) without disturbing the cell aggregate. The retinal organoids were maintained by replacing 100 μL of medium per well with fresh OC-medium every third day until the optic cups were used at Day 21 after seeding.

Liposome Uptake in Retinal Organoids. For *in vitro* uptake studies, liposomes with the same membrane composition as Lip A, Lip B, and Lip C were prepared adding 0.5 mol % of the fluorescently labeled lipid (DPPE-Atto655). Optic cups at Day 21, were pooled 6 to a well and ∼100 optic cups per formulation were incubated with 400 μM liposomes in OC-medium for 12 h. The 100 aggregates were then collected in a Falcon tube and washed twice with 10 mL of Hanks buffered saline solution (HBSS). Cells were dissociated by adding 10 mL of Trypsin-EDTA 1X (T = 37 °C). Optic cups were mechanically disturbed by pipetting and vortexing periodically, during the 5 min trypsin incubation in a 37 °C heat bath. The trypsin was inhibited by adding an equivalent volume of medium. Cells were then pelleted and resuspended in 500 μL of HBSS before passing through a cell strainer. Cells were fixed by incubation for 30 min on ice in 1.5 mL of 4% paraformaldehyde (Sigma-Aldrich). Cells were washed with 12 mL of PBS and resuspended in 3 mL of blocking buffer; 0.05% Digitonin (5% in water, Invitrogen), 10% goat serum, 0.1% sodium citrate, 1% bovine serum albumin (BSA) in PBS, for 30 min at room temperature. Cells were washed twice with 12 mL of PBS and the pellet was resuspended in appropriate volume of staining buffer. Cells were then divided into a 350 μL microwell plate and incubated with an appropriate amount of primary antibody overnight at 4 °C. Cells were washed three times with PBS and incubated with secondary antibody, (antimouse-Alexa488 or antirabit-Alexa488 (Jackson ImmunoResearch)) for 1 h at room temperature. Cells were washed three times with PBS and resuspended in 250 μL of PBS. Cell uptake was evaluated by flow cytometer on a BD LSR II (BD Bioscience), collecting data in the APC-A and FITC channel, analyzing 10.000 events per sample.

***In Vivo* Efficacy of Liposomes and Progenitor Cell Transplants.** All animal experiments were approved by the Institutional Animal Care and Use Committee (IACUC) at Schepens Eye Research Institute. C57BL/6J (Charles River Laboratories) mice were kept on a 12 h light 12 h dark cycle. Food and water were provided ad libitum. Mice were anesthetized by intraperitoneal (IP) injection of 100−200 mg/kg ketamine and 20 mg/kg xylazine (Accutome). Under anesthesia the mice were given one eye drop of tropicamide and one intravitreal injection of 2 μL of 20 mM *N*-methyl-D-aspartic acid (NMDA) in the right eye, using a 100 μm diameter glass pipet.[94−96] Care was taken not to injure the lens during the procedure. The left eye was kept as contralateral control. After the procedure GenTeal was applied to both eyes. Two h after injection of NMDA, mice were anesthetized by isofluorane inhalation using O_2 as the carrier gas. Mice were then given one 2 μL intravitreal injection of 10 mM liposome suspension of either Lip A, Lip B, or empty Lip C, into the right eye. GenTeal was applied to the injected eye. Four days after NMDA injection, three groups were anesthetized by IP injection of 100−200 mg/kg ketamine and 20 mg/kg xylazine and transplanted with 20 000 GFP^+ transplant RGCs by intravitreal injection of 2 μL of cell suspension in PBS. Four weeks after transplantation ERGs were recorded, mice were euthanized, and eyes were collected.

GFP Expressing RGCs for Transplantations. RGC differentiation, isolation, and selection were performed as described before.[84] Briefly, murine Thy1-GFP iPSCs, kindly provided by the laboratory of Joshua Sanes, were differentiated into retinal tissue in three-dimensional retinal organoids through 21 days culture following the retinal organoid protocol described above. At day 21 aggregates were collected washed with HBSS and dissociated with freshly activated papain in 1.1 mM EDTA, 0.3 mM β-mercaptoethanol, 5.5 mM cysteine-HCl in 50 mL of HBSS preincubated for 30 min at 37 °C, 5% CO_2, 5 mL per 500 aggregates. Aggregates were left in active papain for 3 min, vortexing thoroughly to mechanically dissociate the cells. The cell suspension was then mixed 1:1 with DTI−benzonase and passed through a 40 μm cell strainer. The strainer was washed with an equal volume of DTI−benzonase, and cells were spun down and resuspended in RGC medium (see Supporting Information). GFP^+ RGCs were isolated using magnetic beads (Dynabeads, Invitrogen) with anti-Thy1, following the instructions of the manufacturer. Cells were counted using Trypan-blue staining, suspended in HBSS.

Electroretinography. The function of retinal ganglion cells was assessed by electroretinography (ERG)-scotopic threshold response (STR) using a Diagnosys Espion 3 system with Ganzfield bowl. C57BL/6J mice (Charles River Laboratories) were dark-adapted overnight prior to recordings. The mice were anesthetized by IP injection of 100−200 mg/kg ketamine and 20 mg/kg xylazine and placed on a heating pad to maintain temperature throughout the recordings. Pupils were dilated in both eyes by one drop of tropicamide. GelTal (hypromellose) was applied to the eyes to ensure conduction to the electrodes. The reference electrode (needle) was placed subcutaneously in the forehead and measuring electrodes (gold loops) were placed on the corneas. For the stimulation, a series of white flashes were used at 0.0001, 0.001, 0.01, 0.1, and 5 cd-s/m^2 intensities with mice exposed to 5 flashes per intensity with a 30 s recovery in between each flash. Electroretinograms were recorded with positive STR, negative STR, for which a- and b-waves were analyzed. The STR data shown in this paper were obtained under 0.001 cd-s/m^2 flash intensities while the a-wave and b-wave data were obtained for 0.1 cd-s/m^2. These flash intensities produced electroretinograms with the best signal-to-noise ratio.

Immunohistochemistry and Confocal Imaging. Eyes from euthanized mice were collected in PBS and fixed in 4% PFA overnight.

DOI: 10.1021/acsnano.8b00596
ACS Nano 2018, 12, 7497−7508

Retinas were carefully dissected under a microscope. Retinas were blocked with 10% goat serum overnight at room temperature. Retinas were then washed with 0.1% triton × 0.1% tween 20 in PBS three times before incubation with anti-RBPMS-Rb-IgG (Abcam) and anti-GFP-m-igG (Abcam) overnight at 4 °C. After they were washed three times as described above, the retinas were incubated with antimouse-Alexa647 and antirabit-Alexa488 1 h at room temperature. Lastly the retinas were washed, incubated with 0.5 μg/mL DAPI in PBS for 1 min at room temperature, and washed again before mounting on glass slides using 9% poly vinyl-alcohol, 22% glycerol, 2% 1,4-diazabicyclo[2.2.2]octane in 88 mM Tris-HCl, pH 8.5.

Slides were imaged on a Leica TCS SP5 confocal microscope using a 40× oil emission objective. The predefined settings for the dyes used were chosen in the Leica software. Sequential scanning was used to avoid spillover between the DAPI channel and the Alexa488 channel. Retinas were imaged approximately 1 mm from the optic nerve head. To quantify surviving host RGS, z-stacks of approximately 16 μm with a step size of 0.5 μm were collected. Stacks were *z*-projected to form one image in ImageJ. 2−3 images were obtained per retina. Surviving RGCs were counted manually. To evaluate survival of transplanted RGCs that might be heterogeneously distributed across the retina, the whole retina was imaged using a Zeiss Axio Scan Z.1 slide scanner (20× objective). Signals were recorded in the 488, 560, and 647 nm channels. To eliminate some of the green autofluorescence from the retina, the signal from the 560 nm channel was subtracted from the 488 nm channel before counting the green cells in Zeiss Zen Blue and Black lite software. Cells were counted manually.

Statistical Analysis. Statistical analysis was performed using GraphPad Prism 7 software. The following statistical methods were used to analyze the biological data: (Figure 2A) one-way ANOVA post hoc Tukey HSD test; (Figure 2B) two-way ANOVA; (Figure 3A) one-way ANOVA, no significance; (Figure 3B) one-way ANOVA post hoc Tukey HSD test; (Figure 3C) Kruskal−Wallis, no significance; (Figure 4D) one-way ANOVA post hoc Tukey HSD; (Figure 5A) one-way ANOVA, no significance; (Figure 5B) one-way ANOVA post hoc Tukey HSD test; (Figure 5C) Kruskal−Wallis post hoc Dunn's test; (Figure 6A) One-way ANOVA post hoc Tukey HSD; (Figure 6B) Unpaired *t* test, no significance. The threshold of statistical significance (alpha) for all analyses was 0.05. Distribution curves and quantile−quantile (Q−Q) plots were used to determine whether data sets were parametric or nonparametric. Statistical significance between healthy control eyes and treated eyes was significant and not shown for clarity.

ASSOCIATED CONTENT

Supporting Information

The Supporting Information is available free of charge on the ACS Publications website at DOI: 10.1021/acsnano.8b00596.

Lipopeptide mass spectra and chromatography traces; calcein leakage from liposomes; liposome bioactivity Western blots; flow cytometry scatter plots; electroretinograms; retina micrograms, and cell culture media compositions (PDF)

AUTHOR INFORMATION

Corresponding Author

*E-mail: anur@nanotech.dtu.dk.

ORCID

Petr Baranov: 0000-0002-5526-7058

Andrew J. Urquhart: 0000-0002-5322-0002

Author Contributions

P.B., M.Y., A.Z.E., and A.J.U. conceived the concept and designed the experiments. A.Z.E., P.K., T.L.A., and A.J.U. manufactured liposomes and performed all liposome related analysis. R.E. and A.J.U. synthesized and analyzed lipopeptides. A.Z.E., J.O., F.M., P.B., and M.Y. performed cell culture experiments and cell analysis. A.Z.E., J.O., P.B., and M.Y. performed *in vivo* studies, immunohistology and ERG analysis. A.Z.E. and A.J.U. wrote the manuscript with contributions of all authors. All authors have given approval to the final version of this manuscript.

Notes

The authors declare no competing financial interest.

ACKNOWLEDGMENTS

We would like to thank the Velux Foundation (A.Z.E. and A.J.U.) and Shore Fellowship (P.B.) for financial support. The Animal core and Confocal Imaging facility at the Schepens Eye Research Institute was supported by NIH National Eye Institute Core Grant P30EYE003790. P.B. and M.Y. would like to thank the Laboratory of Joshua Sanes (Harvard University) for kindly providing the Thy1-GFP iPSCs.

REFERENCES

(1) Quigley, H. A.; Broman, A. T. The Number of People with Glaucoma Worldwide in 2010 and 2020. *Br. J. Ophthalmol.* **2006**, *90*, 262−7.

(2) You, Y.; Gupta, V.; Li, J.; Klistorner, A.; Graham, S. Optic Neuropathies: Characteristic Features and Mechanisms of Retinal Ganglion Cell Loss. *Rev. Neurosci.* **2013**, *24*, 301−321.

(3) Quigley, H. A. Neuronal Death in Glaucoma. *Prog. Retinal Eye Res.* **1999**, *18*, 39−57.

(4) Almasieh, M.; Wilson, A. M.; Morquette, B.; Cueva Vargas, J. L.; Di Polo, A. The Molecular Basis of Retinal Ganglion Cell Death in Glaucoma. *Prog. Retinal Eye Res.* **2012**, *31*, 152−181.

(5) Tam, R. Y.; Fuehrmann, T.; Mitrousis, N.; Shoichet, M. S. Regenerative Therapies for Central Nervous System Diseases: a Biomaterials Approach. *Neuropsychopharmacology* **2014**, *39*, 169−188.

(6) Raff, M. C.; Barres, B. A.; Burne, J. F.; Coles, H. S.; Ishizaki, Y.; Jacobson, M. D. Programmed Cell Death and the Control of Cell Survival: Lessons from the Nervous System. *Science* **1993**, *262*, 695−700.

(7) Mey, J.; Thanos, S. Intravitreal Injections of Neurotrophic Factors Support the Survival of Axotomized Retinal Ganglion Cells in Adult Rats *In Vivo*. *Brain Res.* **1993**, *602*, 304−317.

(8) Ward, M. S.; Khoobehi, A.; Lavik, E. B.; Langer, R.; Young, M. J. Neuroprotection of Retinal Ganglion Cells in DBA/2J Mice with GDNF-loaded Biodegradable Microspheres. *J. Pharm. Sci.* **2007**, *96*, 558−568.

(9) Pease, M. E.; Zack, D. J.; Berlinicke, C.; Bloom, K.; Cone, F.; Wang, Y.; Klein, R. L.; Hauswirth, W. W.; Quigley, H. A. Effect of CNTF on Retinal Ganglion Cell Survival in Experimental Glaucoma. *Invest. Ophthalmol. Visual Sci.* **2009**, *50*, 2194−2200.

(10) Zhang, C. W.; Lu, Q.; You, S. W.; Zhi, Y.; Yip, H. K.; Wu, W.; So, K. F.; Cui, Q. CNTF and BDNF Have Similar Effects on Retinal Ganglion Cell Survival but Differential Effects on Nitric Oxide Synthase Expression Soon after Optic Nerve Injury. *Invest. Ophthalmol. Visual Sci.* **2005**, *46*, 1497−1503.

(11) Martin, K. R.; Quigley, H. A.; Zack, D. J.; Levkovitch-Verbin, H.; Kielczewski, J.; Valenta, D.; Baumrind, L.; Pease, M. A.; Klein, R. L.; Hauswirth, W. W. Gene Therapy with Brain-Derived Neurotrophic Factor as a Protection: Retinal Ganglion Cells in a Rat Glaucoma Model. *Invest. Ophthalmol. Visual Sci.* **2003**, *44*, 4357−4365.

(12) Mansour-Robaey, S.; Clarke, D. B.; Wang, Y. C.; Bray, G. M.; Aguayo, A. J. Effects of Ocular Injury and Administration of Brain-Derived Neurotrophic Factor on Survival and Regrowth of Axotomized Retinal Ganglion Cells. *Proc. Natl. Acad. Sci. U. S. A.* **1994**, *91*, 1632−1636.

(13) Parrilla-Reverter, G.; Agudo, M.; Sobrado-Calvo, P.; Salinas-Navarro, M.; Villegas-Perez, M. P.; Vidal-Sanz, M. Effects of Different Neurotrophic Factors on the Survival of Retinal Ganglion Cells after a Complete Intraorbital Nerve Crush Injury: A Quantitative *In Vivo* Study. *Exp. Eye Res.* **2009**, *89*, 32−41.

DOI: 10.1021/acsnano.8b00596
ACS Nano 2018, 12, 7497−7508

(14) Park, K. K.; Liu, K.; Hu, Y.; Kanter, J. L.; He, Z. PTEN/mTOR and Axon Regeneration. *Exp. Neurol.* **2010**, *223*, 45−50.
(15) Sun, F.; Park, K. K.; Belin, S.; Wang, D.; Lu, T.; Chen, G.; Zhang, K.; Yeung, C.; Feng, G.; Yankner, B. A.; He, Z. Sustained Axon Regeneration Induced by Co-Deletion of PTEN and SOCS3. *Nature* **2011**, *480*, 372−375.
(16) Ohtake, Y.; Hayat, U.; Li, S. PTEN Inhibition and Axon Regeneration and Neural Repair. *Neural Regener. Res.* **2015**, *10*, 1363−1368.
(17) Bei, F.; Lee, H. H. C.; Liu, X.; Gunner, G.; Jin, H.; Ma, L.; Wang, C.; Hou, L.; Hensch, T. K.; Frank, E.; Sanes, J. R.; Chen, C.; Fagiolini, M.; He, Z. Restoration of Visual Function by Enhancing Conduction in Regenerated Axons. *Cell* **2016**, *164*, 219−232.
(18) van Adel, B. A.; Arnold, J. M.; Phipps, J.; Doering, L. C.; Ball, A. K. Ciliary Neurotrophic Factor Protects Retinal Ganglion Cells from Axotomy-induced Apoptosis *via* Modulation of Retinal Glia *In Vivo*. *J. Neurobiol.* **2005**, *63*, 215−234.
(19) Ji, J. Z.; Elyaman, W.; Yip, H. K.; Lee, V. W.; Yick, L. W.; Hugon, J.; So, K. F. CNTF Promotes Survival of Retinal Ganglion Cells after Induction of Ocular Hypertension in Rats: The Possible Involvement of STAT3 Pathway. *Eur. J. Neurosci.* **2004**, *19*, 265−272.
(20) Leaver, S. G.; Cui, Q.; Plant, G. W.; Arulpragasam, A.; Hisheh, S.; Verhaagen, J.; Harvey, A. R. AAV-Mediated Expression of CNTF Promotes Long-Term Survival and Regeneration of Adult Rat Retinal Ganglion Cells. *Gene Ther.* **2006**, *13*, 1328−1341.
(21) Müller, A.; Hauk, T. G.; Leibinger, M.; Marienfeld, R.; Fischer, D. Exogenous CNTF Stimulates Axon Regeneration of Retinal Ganglion Cells Partially *via* Endogenous CNTF. *Mol. Cell. Neurosci.* **2009**, *41*, 233−246.
(22) Yokogami, K.; Wakisaka, S.; Avruch, J.; Reeves, S. A. Serine Phosphorylation and Maximal Activation of STAT3 during CNTF Signaling Is Mediated by the Rapamycin Target mTOR. *Curr. Biol.* **2000**, *10*, 47−50.
(23) Leibinger, M.; Müller, A.; Andreadaki, A.; Hauk, T. G.; Kirsch, M.; Fischer, D. Neuroprotective and Axon Growth-Promoting Effects Following Inflammatory Stimulation on Mature Retinal Ganglion Cells in Mice Depend on Ciliary Neurotrophic Factor and Leukemia Inhibitory Factor. *J. Neurosci.* **2009**, *29*, 14334−14341.
(24) Le Roith, D.; Butler, A. A. Insulin-like Growth Factors in Pediatric Health and Disease. *J. Clin. Endocrinol. Metab.* **1999**, *84*, 4355−4361.
(25) Laplante, M.; Sabatini, D. M. mTOR Signaling at a Glance. *J. Cell Sci.* **2009**, *122*, 3589−3594.
(26) Dupraz, S.; Grassi, D.; Karnas, D.; Nieto Guil, A. F.; Hicks, D.; Quiroga, S. The Insulin-like Growth Factor 1 Receptor Is Essential for Axonal Regeneration in Adult Central Nervous System Neurons. *PLoS One* **2013**, *8*, e54462.
(27) Joshi, Y.; Sória, M. G.; Quadrato, G.; Inak, G.; Zhou, L.; Hervera, A.; Rathore, K. I.; Einaggar, M.; Currhiarini, M.; Marine, J. C.; Puttagunta, R.; Di Giovanni, S. The MDM4/MDM2-p53-IGF1 Axis Controls Axonal Regeneration, Sprouting and Functional Recovery after CNS Injury. *Brain* **2015**, *138*, 1843−1862.
(28) Hwang, S. M.; Lopez, C. A.; Heck, D. E.; Gardner, C. R.; Laskin, D. L.; Denhardt, D. T. Osteopontin Inhibits Induction of Nitric Oxide Synthase Gene Expression by Inflammatory Mediators in Mouse Kidney Epithelial Cells. *J. Biol. Chem.* **1994**, *269*, 711−715.
(29) Denhardt, D. T.; Noda, M.; O'Regan, A. W.; Pavlin, D.; Berman, J. S. Osteopontin as a Means to Cope with Environmental Insults: Regulation of Inflammation, Tissue Remodeling, and Cell Survival. *J. Clin. Invest.* **2001**, *107*, 1055−1061.
(30) Meller, R.; Stevens, S. L.; Minami, M.; Cameron, J. A.; King, S.; Rosenzweig, H.; Doyle, K.; Lessov, N. S.; Simon, R. P.; Stenzel-Poore, M. P. Neuroprotection by Osteopontin in Stroke. *J. Cereb. Blood Flow Metab.* **2005**, *25*, 217−225.
(31) Duan, X.; Qiao, M.; Bei, F.; Kim, I. J.; He, Z.; Sanes, J. R. Subtype-Specific Regeneration of Retinal Ganglion Cells Following Axotomy: Effects of Osteopontin and mTOR Signaling. *Neuron* **2015**, *85*, 1244−1256.
(32) Park, K.; Liu, K.; Hu, Y.; Smith, P. D.; Wang, C.; Cai, B.; Xu, B.; Connolly, L.; Kramvis, I.; Sahin, M.; He, Z. Promoting Axon Regeneration in the Adult CNS by Modulation of the PTEN/mTOR Pathway. *Science* **2008**, *322*, 963−966.
(33) Liu, K.; Lu, Y.; Lee, J. K.; Samara, R.; Willenberg, R.; Sears-Kraxberger, I.; Tedeschi, A.; Park, K. K.; Jin, D.; Cai, B.; Xu, B.; Connolly, L.; Steward, O.; Zheng, B.; He, Z. PTEN Deletion Enhances the Regenerative Ability of Adult Corticospinal Neurons. *Nat. Neurosci.* **2010**, *13*, 1075−1081.
(34) Kompella, U. B.; Amrite, A. C.; Pacha Ravi, R.; Durazo, S. A. Nanomedicines for Back of the Eye Drug Delivery, Gene Delivery, and Imaging. *Prog. Retinal Eye Res.* **2013**, *36*, 172−198.
(35) Bochot, A.; Fattal, E. Liposomes for Intravitreal Drug Delivery: A State of the Art. *J. Controlled Release* **2012**, *161*, 628−634.
(36) Zhang, R.; He, R.; Qian, J.; Guo, J.; Xue, K.; Yuan, Y. F. Treatment of Experimental Autoimmune Uveoretinitis with Intravitreal Injection of Tacrolimus (FK506) Encapsulated in Liposomes. *Invest. Ophthalmol. Visual Sci.* **2010**, *51*, 3572−3582.
(37) Zeng, S.; Hu, C.; Wei, H.; Lu, Y.; Zhang, Y.; Yang, J.; Yun, G.; Zou, W.; Song, B. Intravitreal Pharmacokinetics of Liposome-Encapsulated Amikacin in a Rabbit Model. *Ophthalmology* **1993**, *100*, 1640−1644.
(38) Wang, Y.; Rajala, A.; Cao, B.; Ranjo-Bishop, M.; Agbaga, M.-P.; Mao, C.; Rajala, R. V. S. Cell-Specific Promoters Enable Lipid-Based Nanoparticles to Deliver Genes to Specific Cells of the Retina. *Theranostics* **2016**, *6*, 1514−1527.
(39) Rajala, A.; Wang, Y.; Zhu, Y.; Ranjo-Bishop, M.; Ma, J.-X.; Mao, C.; Rajala, R. V. S. Nanoparticle-Assisted Targeted Delivery of Eye-Specific Genes to Eyes Significantly Improves the Vision of Blind Mice *In Vivo*. *Nano Lett.* **2014**, *14*, 5257−5263.
(40) Tan, M. L.; Choong, P. F.; Dass, C. R. Recent Developments in Liposomes, Microparticles and Nanoparticles for Protein and Peptide Drug Delivery. *Peptides* **2010**, *31*, 184−193.
(41) Allen, T. M.; Cullis, P. R. Liposomal Drug Delivery Systems: From Concept to Clinical Applications. *Adv. Drug Delivery Rev.* **2013**, *65*, 36−48.
(42) Johnsen, K. B.; Moos, T. Revisting Nanoparticle Technology for Blood-Brain Barrier Transport: Unfolding at the Endothelial Gate Improves the Fate of Transferrin Receptor-Targeted Liposomes. *J. Controlled Release* **2016**, *222*, 32−46.
(43) Takeda, Y. S.; Xu, Q. Synthetic and Nature-Derived Lipid Nanoparticles for Neural Regeneration. *Neural Regener. Res.* **2015**, *10*, 689−690.
(44) García-Recio, M.; Cladera, A.; Bento, L.; Dominguez, J.; de Gracia, S. R.; Sartori, F.; Del Campo, R.; García, L.; Ballester, C.; Gines, J.; Bargay, J.; Sampol, A.; Gutiérrez, A. Analysis of the Role of Intratecal Liposomal Cytarabine in the Prophylaxis and Treatment of Central Nervous System Lymphomatosis: The Balearic Lymphoma Group Experience. *PLoS One* **2017**, *12*, e0179595.
(45) da Gruz, M. T.; Cardoso, A. L.; de Almeida, L. P.; Simões, S.; de Lima, M. C. Tf-Lipoplex-Mediated NGF Gene Transfer to the CNS: Neuronal Protection and Recovery in an Excitotoxic Model of Brain Injury. *Gene Ther.* **2005**, *12*, 1242−1252.
(46) Lu, K. W.; Chen, Z. Y.; Jin, D. D.; Hou, T. S.; Cao, L.; Fu, Q. Cationic Lipsome-Mediated GDNF Gene Transfer after Spinal Cord Injury. *J. Neurotrauma* **2002**, *19*, 1081−1090.
(47) Popovich, P. G.; Guan, Z.; Huitinga, I.; van Rooijen, N.; Stokes, B. T. Depletion of Hematogenous Macrophages Promotes Partial Hindlimb Recovery and Neuroanatomical Repair after Experimental Spinal Cord Injury. *Exp. Neurol.* **1999**, *158*, 351−365.
(48) Singh, K.; Balligand, J. L.; Fischer, T. A.; Smith, T. W.; Kelly, R. A. Glucocorticoids Increase Osteopontin Expression in Cardiac Myocytes and Microvascular Endothelial Cells Role in Regulation of Inducible Nitric Oxide Synthase. *J. Biol. Chem.* **1995**, *270*, 28471−28478.
(49) Miyauchi, A.; Alvarez, J.; Greenfield, E. M.; Teti, A.; Grano, M.; Colucci, S.; Zambonin-Zallone, A.; Ross, P. F.; Teitelbaum, S. L.; Cheresh, D.; Hruska, K. A. Recognition of Osteopontin and Related

DOI: 10.1021/acsnano.8b00596
ACS Nano 2018, 12, 7497−7508

Peptides by an Alpha v Beta 3 Integrin Stimulates Immediate Cell Signals in Osteoclasts. *J. Biol. Chem.* **1991**, *266*, 20369−20374.
(50) Ohtake, Y.; Park, D.; Abdul-Muneer, P. M.; Li, H.; Xu, B.; Sharma, K.; Smith, G. M.; Selzer, M. E.; Li, S. The Effect of Systemic PTEN Antagonist Peptides on Axon Growth and Functional Recovery after Spinal Cord Injury. *Biomaterials* **2014**, *35*, 4610−4626.
(51) Nel, A. E.; Mädler, L.; Velegol, D.; Xia, T.; Hoek, E. M.; Somasundaran, P.; Klaessig, F.; Castranova, V.; Thompson, M. Understanding Biophysicochemical Interactions at the Nano-Bio Interface. *Nat. Mater.* **2009**, *8*, 543−557.
(52) Filion, M. C.; Phillips, N. C. Toxicity and Immunomodulatory Activity of Liposomal Vectors Formulated with Cationic Lipids toward Immune Effector Cells. *Biochim. Biophys. Acta, Biomembr.* **1997**, *1329*, 345−356.
(53) Eriksen, A. Z.; Brewer, J.; Andresen, T. L.; Urquhart, A. J. The Diffusion Dynamics of PEGylated Liposomes in the Intact Vitreous of the *Ex Vivo* Porcine Eye: A Fluorescence Correlation Spectroscopy and Biodistribution Study. *Int. J. Pharm.* **2017**, *522*, 90−97.
(54) Kim, C. E.; Lim, S. K.; Kim, J. S. *In Vivo* Antitumor Effect of Cromolyn in PEGylated Liposomes for Pancreatic Cancer. *J. Controlled Release* **2012**, *157*, 190−195.
(55) Begum, M.; Abbulu, K.; Sudhakar, M. Flurbiprofen-Loaded Stealth Liposomes: Studies on the Development, Characterization, Pharmacokinetics, and Biodistribution. *J. Young Pharm.* **2012**, *4*, 209−19.
(56) Kontogiannopoulos, K. N.; Tsermentseli, S. K.; Assimopoulou, A. N.; Papageorgiou, V. P. Sterically Stabilized Liposomes as a Potent Carrier for Shikonin. *J. Liposome Res.* **2014**, *24*, 230−240.
(57) Wong, V.; Pearsall, D.; Arriaga, R.; Ip, N. Y.; Stahl, N.; Lindsay, R. M. Binding Characteristics of Ciliary Neurotrophic Factor to Sympathetic Neurons and Neuronal Cell Lines. *J. Biol. Chem.* **1995**, *270*, 313−318.
(58) Waldbillig, R. J.; Arnold, D. R.; Fletcher, R. T.; Chader, G. J. Insulin and IGF-1Binding in Chick Sclera. *Invest. Ophthalmol. Visual Sci.* **1990**, *31*, 1015−1022.
(59) McGill, T. J.; Prusky, G. T.; Douglas, R. M.; Yasumura, D.; Matthes, M. T.; Nune, G.; Donohue-Rolfe, K.; Yang, H.; Niculescu, D.; Hauswirth, W. W.; Girman, S. V.; Lund, R. D.; Duncan, J. L.; LaVail, M. M. Intraocular CNTF Reduces Vision in Normal Rats in a Dose-Dependent Manner. *Invest. Ophthalmol. Visual Sci.* **2007**, *48*, 5756−5766.
(60) Eiraku, M.; Sasai, Y. Mouse Embryonic Stem Cell Culture for Generation of Three-Dimensional Retinal and Cortical Tissues. *Nat. Protoc.* **2011**, *7*, 69−79.
(61) Fey, S. J.; Wrzesinski, K. Determination of Drug Toxicity Using 3D Spheroids Constructed from an Immortal Human Hepatocyte Cell Line. *Toxicol. Sci.* **2012**, *127*, 403−411.
(62) Lukowski, J. K.; Weaver, E. M.; Hummon, A. B. Analyzing Liposomal Drug Delivery Systems in Three-Dimensional Cell Culture Models Using MALDI Imaging Mass Spectrometry. *Anal. Chem.* **2017**, *89*, 8453−8458.
(63) Baranov, P.; Lin, H.; McCabe, K.; Gale, D.; Cai, S.; Lieppman, B.; Morrow, D.; Lei, P.; Liao, J.; Young, M. A Novel Neuroprotective Small Molecule for Glial Cell Derived Neurotrophic Factor Induction and Photoreceptor Rescue. *J. Ocul. Pharmacol. Ther.* **2017**, *33*, 412−422.
(64) Torres, A. G.; Gait, M. J. Exploiting Cell Surface Thiols to Enhance Cellular Uptake. *Trends Biotechnol.* **2012**, *30*, 185−190.
(65) Guenther, E.; Schmid, S.; Grantyn, R.; Zrenner, E. *In Vitro* Identification of Retinal Ganglion Cells in Culture without the Need of Dye Labeling. *J. Neurosci. Methods* **1994**, *51*, 177−181.
(66) Ricketts, K. P.; Cheema, U.; Nyga, A.; Castoldi, A.; Guazzoni, C.; Magdeldin, T.; Emberton, M.; Gibson, A. P.; Royle, G. J.; Loizidou, M. A 3D *In Vitro* Cancer Model as a Platform for Nanoparticle Uptake and Imaging Investigations. *Small* **2014**, *10*, 3954−3961.
(67) López-Dávila, V.; Magdeldin, T.; Welch, H.; Dwek, M. V.; Uchegbu, I.; Loizidou, M. Efficacy of DOPE/DC-Cholesterol Liposomes and GCPQ Micelles as AZD6244 Nanocarriers in a 3D Colorectal Cancer *In Vitro* Model. *Nanomedicine* **2016**, *11*, 331−344.
(68) Colley, H. E.; Hearnden, V.; Avila-Olias, M.; Cecchin, D.; Canton, I.; Madsen, J.; MacNeil, S.; Warren, N.; Hu, K.; McKeating, J. A.; Armes, S. P.; Murdoch, C.; Thornhill, M. H.; Battaglia, G. Polymersome-Mediated Delivery of Combination Anticancer Therapy to Head and Neck Cancer Cells: 2D and 3D *In Vitro* Evaluation. *Mol. Pharmaceutics* **2014**, *11*, 1176−1188.
(69) Rodriguez, A. R.; de Sevilla Müller, L. P.; Brecha, N. C. The RNA Binding Protein RBPMS is a Selective Marker of Ganglion Cells in the Mammalian Retina. *J. Comp. Neurol.* **2014**, *522*, 1411−1443.
(70) Johansson, U. E.; Eftekhari, S.; Warfvinge, K. A Battery of Cell- and Structure- Specific Markers for the Adult Porcine Retina. *J. Histochem. Cytochem.* **2010**, *58*, 377−389.
(71) Lam, T. T.; Abler, A. S.; Kwong, J. M.; Tso, M. O. N-Methyl-D-Aspartate (NMDA) induced Apoptosis in Rat Retina. *Exp. Eye Res.* **1999**, *40*, 2391−2397.
(72) Ohno, Y.; Nakanishi, T.; Umigai, N.; Tsuruma, K.; Shimazawa, M.; Hara, H. Oral Administration of Crocetin Prevents Inner Retinal Damage Induced by N-Methyl-D-Aspartate in Mice. *Eur. J. Pharmacol.* **2012**, *690*, 84−89.
(73) Stout, A. K.; Raphael, H. M.; Kanterewicz, B. I.; Klann, E.; Reynolds, I. J. Glutamate-Induced Neuron Death Requires Mitochondrial Calcium Uptake. *Nat. Neurosci.* **1998**, *1*, 366−373.
(74) Kuehn, S.; Rodust, C.; Stute, G.; Grotegut, P.; Meißner, W.; Reinehr, S.; Dick, H. B.; Joachim, S. C. Concentration-Dependent Inner Retina Layer Damage and Optic Nerve Degeneration in a NMDA Model. *J. Mol. Neurosci.* **2017**, *63*, 283−299.
(75) Smith, B.; Wang, X.; Chauhan, B.; Côté, P.; Tremblay, F. Contribution of Retinal Ganglion Cells to the Mouse Electroretinogram. *Doc. Ophthalmol.* **2014**, *128*, 155−168.
(76) Germain, F.; Istillarte, M.; Gómez-Vicente, V.; Pérez-Rico, C.; de la Villa, P. Electroretinographical and Histological Study of Mouse Retina after Optic Nerve Section: A Comparison between Wild-type and Retinal Degeneration 1 Mice. *Clin. Exp. Ophthalmol.* **2013**, *41*, 593−602.
(77) Robson, J. G.; Maeda, H.; Saszik, S. M.; Frishman, L. P. *In Vivo* Studies of Signaling in Rod Pathways of the Mouse Using the Electroretinogram. *Vision Res.* **2004**, *44*, 3253−3268.
(78) Chintala, S.; Cheng, M.; Zhang, X. Decreased Expression of DREAM Promotes the Degeneration of Retinal Neurons. *PLoS One* **2015**, *10*, e0127776.
(79) Reynolds, A. L.; Farrar, G. J.; Humphries, P.; Kenna, P. F. Variation in the Electroretinogram of C57BL/6 Substrains of Mouse. *Recent Advances in Retinal Degeneration*; Anderson, R. E., LaVail, M. M., Hollyfield, J. G., Eds.; Springer: New York, 2008; pp 383−391.
(80) Porciatti, V. Electrophysiological Assessment of Retinal Ganglion Cell Function. *Exp. Eye Res.* **2015**, *141*, 164−170.
(81) Saszik, S. M.; Robson, J. G.; Frishman, L. J. The Scotopic Threshold Response of the Dark-adapted Electroretinogram of the Mouse. *J. Physiol.* **2002**, *543*, 899−916.
(82) Manabe, S.; Lipton, S. A. Divergent NMDA Signals Leading to Proapoptotic and Antiapoptotic Pathways in the Rat Retina. *Invest. Ophthalmol. Visual Sci.* **2003**, *44*, 385−392.
(83) McKinnon, S. J.; Schlamp, C. L.; Nickells, R. W. Mouse Models of Retinal Ganglion Cell Death and Glaucoma. *Exp. Eye Res.* **2009**, *88*, 816−824.
(84) Minelli, T.; Oswald, J.; Young, M.; Baranov, P. Differentiation and Transplantation of IPSc Derived Mouse Retinal Ganglion Cells. *Cell Transplant.* **2018**, under review.
(85) Sakaguchi, D. S.; Van Hoffelen, S. J.; Theusch, E.; Parker, E.; Orasky, J.; Harper, M. M.; Benediktsson, A.; Young, M. J. Transplantation of Neural Progenitor Cells into the Developing Retina of the Brazilian Opossum: An *In Vivo* System for Studying Stem/Progenitor Cell Plasticity. *Dev. Neurosci.* **2005**, *26*, 336−345.
(86) Hertz, J.; Qu, B.; Hu, Y.; Patel, R. D.; Valenzuela, D. A.; Goldberg, J. L. Survival and Integration of Developing and Progenitor-Derived Retinal Ganglion Cells Following Transplantation. *Cell Transplant.* **2014**, *23*, 855−872.

DOI: 10.1021/acsnano.8b00596
ACS Nano 2018, 12, 7497−7508

(87) Dyer, M. A. An Eye on Retinal Recovery. *Nature* **2016**, *540*, 350−351.
(88) Singhal, S.; Lawrence, J. M.; Salt, T. E.; Khaw, P. T.; Limb, G. A. Triamcinolone Attenuates Macrophage/microglia Accumulation Associated with NMDA-Induced RGC Death and Facilitates Survival of Müller Stem Cell Grafts. *Exp. Eye Res.* **2010**, *90*, 308−315.
(89) Ma, J.; Kabiel, M.; Tucker, B. A.; Ge, J.; Young, M. J. Combining Chondroitinase ABC and Growth Factors Promotes the Integration of Murine Retinal Progenitor Cells Transplanted into Rho(−/−) Mice. *Mol. Vision* **2011**, *17*, 1759−1770.
(90) Sun, Y.; Williams, A.; Waisbourd, M.; Iacovitti, L.; Katz, L. J. Stem Cell Therapy for Glaucoma: Science or Snake Oil? *Surv. Ophthalmol.* **2015**, *60*, 93−105.
(91) Wang, X.; Jiang, C.; Liu, M.; Yang, Z.; Liu, C.; Qin, L.; Peng, Q. Transplanted Retinal Progenitor Cells Exhibit Long-Term Survival and Function in a Murine Model of Laser Photocoagulation. *Int. J. Clin. Exp. Pathol.* **2016**, *9*, 5510−5514.
(92) Bruun, J.; Larsen, T. B.; Jølck, R. I.; Eliasen, R.; Holm, R.; Gjetting, T.; Andresen, T. L. Investigation of Enzyme-Sensitive Lipid Nanoparticles for Delivery of siRNA to Blood−brain Barrier and Glioma Cells. *Int. J. Nanomed.* **2015**, *10*, 5995−6008.
(93) Xu, X.; Costa, A.; Burgess, D. J. Protein Encapsulation in Unilamellar Liposomes: High Encapsulation Efficiency and a Novel Technique to Assess Lipid-Protein Interaction. *Pharm. Res.* **2012**, *29*, 1919−1931.
(94) Laabich, A.; Li, G.; Cooper, N. G. Characterization of Apoptosis-Genes Associated with NMDA Mediated Cell Death in the Adult Rat Retina. *Mol. Brain Res.* **2001**, *91*, 34−42.
(95) Hara, A.; Niwa, M.; Kumada, M.; Aoki, H.; Kunisada, T.; Oyama, T.; Yamamoto, T.; Kozawa, O.; Mori, H. Intraocular Injection of Folate Antagonist Methotrexate Induces Neuronal Differentiation of Embryonic Stem Cells Transplanted in the Adult Mouse Retina. *Brain Res.* **2006**, *1085*, 33−42.
(96) Zhao, L.; Chen, G.; Li, J.; Fu, Y.; Mavlyutov, T.; Yao, A.; Nickells, R.; Gong, S.; Guo, L. W. An Intraocular Drug Delivery System Using Targeted Nanocarriers Attenuates Retinal Ganglion Cell Degeneration. *J. Controlled Release* **2017**, *247*, 153−166.

DOI: 10.1021/acsnano.8b00596
ACS Nano 2018, 12, 7497−7508